Surfaces and Interfaces 48 (2024) 104241

Contents lists available at ScienceDirect

Surfaces and Interfaces

journal homepage: www.sciencedirect.com/journal/surfaces-and-interfaces

Upcycling of cotton waste to functional carbon dots: Photocatalysis and antibacterial action under vis-NIR light

Evie L. Papadopoulou [a,2,*], Aurelio Barbetta [a,1], Fabrizio Fiorentini [a], Martina Lenzuni [a], Riccardo Carzino [a], Silvia Dante [b], Luca Leoncino [c], Athanassia Athanassiou [a,*]

[a] Smart Materials Group, Istitituto Italiano di Tecnologia, 16163 Genova, Italy
[b] Materials Characterization Facility, Istituto Italiano di Tecnologia, 16163 Genova, Italy
[c] Electron Microscopy Facility, Istituto Italiano di Tecnologia, via Morego 30, Genova 16163, Italy

ARTICLE INFO

Keywords:
Carbon dots
Cotton waste
Fluorescence
Paper sensors
Antibacterial
Photocatalysis

ABSTRACT

Carbon dots are fluorescent nanomaterials with interesting optical properties and good biocompatibility that can be fabricated from many carbon sources. In the present work, we have produced carbon dots from non-woven cotton waste, following an ecological strategy, easy to scale up. The fabricated carbon dots possess strong photoluminescence (PL), they are chemically very stable and biocompatible. We have investigated their photocatalytic properties under visible–near IR light irradiation, and consequently their antibacterial properties under these conditions, using as a model cell the Gram-negative bacteria *Escherichia coli* (*E.coli*). Finally, we have fabricated a proof-of-concept paper sensor by functionalizing lab filter paper with the produced carbon dots, using poly(vinyl alcohol) as binder. The analysis of digital photographs of the paper sensors under UV light reveals a quenching of the photoluminescence of the carbon dots in the presence of *E. coli*, extending the potential applications of carbon dots to paper-based bacterial sensors.

1. Introduction

Carbon dots (CDs) are a relatively new kind of nanomaterial [1,2] that has attracted great attention in recent years due to a set of properties that makes them desirable for many applications. They are carbon-based fluorescent nanomaterials with diameter smaller than 10 nm, good photostability, chemical stability and biocompatibility. They are easily dispersed in water and can be easily functionalized, and their fabrication is generally inexpensive [3,4]. These characteristics make them desirable for applications such as fluorescent sensors [5] for metal ions [6,7], organic solvents [8] and inorganic nanoparticles [9], light emitted devices [10], cell imaging [11,12], photocatalysis [13–15] etc.

Despite that the controllable synthesis of CDs is still in its infancy, one of their biggest advantages is that they can be produced using facile methods, not requiring expensive equipment, such as pyrolysis or solvothermal treatment [3,16], from any source containing carbon, including biomass waste. Biomass waste includes food waste, such as peels and leaves, or other waste coming from consumer or industrial activities, such as fabrics [3], and is most often discarded. However, biomass waste is a low-cost carbon source that can be upcycled to create added-value materials [17]. To this end, CDs have been produced from a variety of carbon sources, such as orange juice [11], cotton [18], yeast [19], brown sugar [8], rice [20], food waste [21] or magnolia flowers [22].

Recently, CDs have emerged as excellent photosensitizers [23] due to their fluorescent and photocatalytic properties. Thus, they have been used to enhance the photocatalytic properties of semiconducting nanoparticles that suffer from fast electron–hole recombination rates and low activity under visible light, by the fabrication of hybrid carbon dot – semiconductor nanostructures [24–27]. However, few reports exist where carbon dots are used as stand-alone photocatalysts for pollutants' removal [14,15,28,29].

The generation of electrons and holes that takes place upon irradiation of a photocatalyst, results in the production of reactive oxygen species (ROS), such as hydroxyl radicals (OH•) and superoxides (O_2^-), which are able to cause oxidative stress in bacteria, perforation of the

* Corresponding authors at: Smart Material Group, Istituto Italiano di Tecnologia, via Morego 30, 16163 Italy.
E-mail addresses: paraskevi.papadopoulou@iit.it (E.L. Papadopoulou), athanassia.athanassiou@iit.it (A. Athanassiou).
[1] Present address: Istituto per lo studio dei materiali nanostrutturati (ISMN) – CNR, Strada Provinciale 35/d n. 9, 00010 Montelibretti (RM)
[2] BeDimensional S.p.A., Lungotorrente Secca 30R, Genova 16163, Italy

https://doi.org/10.1016/j.surfin.2024.104241
Received 19 September 2023; Received in revised form 20 December 2023; Accepted 24 March 2024
Available online 27 March 2024

cell wall, and elimination of intracellular components, leading to cell death [30,31]. Hence, CDs have also emerged as very attractive antimicrobial agents for photodynamic inactivation (PDI) of pathogens, a method that is considered a great promise against antimicrobial resistance [32,33]. PDI relies on the irradiation of pathogens in the presence of photosensitizers, using light with the appropriate wavelength to excite the photosensitizers and cause the consequent production of ROS. However, most photosensitizers absorb light and thus act photocatalytically only under UV irradiation. This is a disadvantage because UV light can be absorbed by most biological samples. In previous works, CDs that have been used for bacteria killing under visible light irradiation were functionalized either with 2,2′-(Ethylenedioxy)bis(ethylamine) (EDA) [34,35] or with ampicillin [36]. The use of visible light was attributed either to the broad absorption spectrum covering the visible region or not discussed.

Herein, we have produced CDs from waste cotton (cotton waste carbon dots, CWCDs) via a simple carbonization process of different non-woven waste materials. These include heterogeneous cotton threads of different sizes and densities. In order to homogenize the carbonization process of the different fabrics, we have dissolved them in an appropriate solvent system, prior to carbonization. We demonstrate that the produced CWCDs, have strong PL properties and they exhibit photocatalytic activity under visible-NIR light irradiation. Furthermore, the CWCDs have been proven antibacterial against the Gram-negative *Escherichia coli* (*E. coli*), under visible-NIR light irradiation. Nevertheless, CWCDs maintain their biocompatible nature when in contact with healthy cells, even under visible-NIR light irradiation for several hours. Finally, a paper sensor has been fabricated, based on the fluorescence of the CWCDs, which quenches in the presence of bacteria. Hence, we demonstrate how the optical characteristics of CWCDs lead to a multifunctional action of the CWCDs for killing and detecting Gram-negative bacteria.

2. Experimental methods

2.1. Materials

waste cotton fibers with a title between 140 and 220 mTex and waste spun cotton with a title between 3 and 300 Ne were obtained from local suppliers (Genova, IT). Acetic anhydride, acetic acid, and sulfuric acid were purchased from Sigma Aldrich and used without further purification. Polyvinyl alcohol (PVA, Mw 146,000–186,000) was purchased from Sigma Aldrich. Filter paper was purchased from Whatman. MilliQ water was used as a solvent. Dialysis membrane (Spectra/Por® 3) was purchased from Fisher Scientific.

2.2. CWCD preparation

Cotton waste material, derived from different phases of the spinning process, spun or unspun, was cut to pieces between 0.1 and 300.0 μm, in order to increase the available surface area for the subsequent dissolution. The obtained powder was dried at 100 °C for 1 h to reduce the adsorbed humidity in the fibers, resulting in a weight loss after drying of ca. 5 %. The material was then dissolved at $T = 50$ °C via esterification. 5 g of the dried cotton powder were immersed in 60 mL of acetic acid to activate the swelling of the fibers and increase their available active surface area. After 1 h, 20.00 mL acetic anhydride and 0.25 mL of sulphuric acid that acted as a catalyst were added to acetylize the hydroxyl groups of the anhydroglucose monomers of cotton's cellulose, thus dissolving the acetylated cellulose. The solution was left under 300 rpm magnetic stirring for 23 h, until complete dissolution. The obtained solution was poured in a glass Petri dish (diameter 10 cm) for solvent evaporation under ambient conditions.

Carbonization of the product was performed in a furnace, following solvent evaporation, by setting a temperature ramp to 200 °C, at a speed of 1 °C/min, and keeping the temperature at 200 °C for 2 h. The samples were collected from the furnace after the temperature was decreased back to room temperature, and they were crumbled with a mortar. Subsequently, ultrapure water (Milli-Q, 18.2 MΩ•cm) was added to the carbonized product and the mixture was tip sonicated (Sonics, Vibra cell, VC750, 750 W max, 30 % of power used) at ambient temperature, for ~3 h, in order to form the CWCDs. First, the insoluble carbon residues were filtered using a 0.2 μm filter membrane. Then, the aqueous dispersion of CWCDs underwent dialysis using a dialysis membrane of 3.5 kDa, for 72 h, changing the water twice a day, resulting in ultrafine CWCDs [37]. The CWCD aqueous dispersion was then centrifuged (12, 000 rpm, 30 min) and the supernatant containing the CWCDs was selected for the work herein. The purified CWCDs were adjusted to a concentration of ~3 mg/mL.

2.3. Characterization

Absorption curves were taken using a UV–visible spectrophotometer (CARY200 Scan, Varian). Photoluminescence (PL) was measured by a Fluorimeter (Horiba). A UV lamp (analytikjena, UVP UVGL-58, 6 Watt) was used to illuminate the fluorescence of the specimens and photographs were taken by digital camera and analyzed with ImageJ [38].

X-ray photoelectron spectroscopy (XPS) was performed using an electron spectrometer (Lab2, Specs, Germany) equipped with a monochromatic X-ray source (1486 eV) and a hemispherical energy analyzer (Phoibos, HSA3500, Specs, Germany). The applied voltage of the Al Kα X-ray source was set at 13 kV and the applied current at 8 mA. The pressure in the analysis chamber was $\sim 1 \times 10^{-9}$ mbar. The large area lens mode was used for both wide and narrow scans. For the wide scan, the energy pass was 90 eV and the energy step was 1 eV. For the narrow high-resolution scan, the energy pass was 30 eV and the energy step was 0.1 eV. A flood gun was used to neutralize the surface charge, having an energy of 7 eV and a filament current of 2.2 A. XPS samples were prepared with carbon dots deposited on indium substrate.

The μRaman spectra (Renishaw Invia, UK) were collected at ambient conditions, with a 514 nm laser excitation line, in backscattering geometry through a 100× objective lens of a microscope (numerical aperture 0.75) used to excite the specimens, at a power of 0.4 mW. A grating with 2400 lines/mm was used. The spectral region scanned was 1000−3000 cm^{-1}, at a spectral resolution of ~1 cm^{-1}.

Small angle X-ray scattering (SAXS) experiments were carried out in transmission geometry by using a Malvern PANalytical third generation Empyrean multipurpose platform. Cu kα radiation (λ=1.54 Å) was used (40 kV, 45 mA). 1D-SAXS measurements were carried out in a vacuum path chamber (Scatter X78) using a beam with line collimation and a GaliPIX3D detector. Quartz capillary (Hilgenberg, DE) with a 1 mm diameter (100 μL volume) was used. Background measurement of ultrapure pure water was performed in the same capillary used for the CWCD dispersion. Scans were performed in the q region 0.1–5.0 nm^{-1} with step size 0.014°, with an exposure time of 30 min. The data analysis was performed using the EasySAXS software (Malvern-PANalytical). The software performs primary data handling steps, such as absorption correction, background-subtraction, and conversion of the scattering angle 2θ to the scattering vector q. Determination of nanoparticle distribution was done by an indirect integral transform technique that relates experimental SAXS data to the volume distribution function Dv(R) using a regularization procedure.

Scanning electron microscopy (SEM; JSM-6490LA, JEOL) analyses were performed, at 10 kV acquiring the signal from secondary electron detector.

Transmission electron microscopy (TEM) was performed using a JEM-1400Plus, with thermionic source (LaB6), operated at 120 kV. 30 μL of the CWCD suspension was deposited on an ultrathin C-film on holey/Cu grid, previously cleaned by plasma (Gatan Solarus 950, O_2 and Ar, 15 W forward RF target power, 1 min).

2.4. Photocatalytic degradation of MB under visible-NIR light

The photocatalytic performance of the CWCDs was investigated by performing photodegradation of aqueous solutions of methylene blue (MB @10 mg/L), containing the CWCDs, under the visible-NIR light of a Xenon lamp (Hamamatsu L9588, 200 W). CWCDs and MB solutions were adequately mixed to reach final CWCD concentrations either 40 mg/mL or 600 mg/mL (named CWCD40 and CWCD600, respectively). The solutions were kept in the dark for at least 1 h before starting the irradiation, in order to reach the adsorption/desorption equilibrium of the dye on the surface of the CWCDs. The distance between the lamp and the sample was 17 cm. The MB degradation was estimated by measuring the MB absorption in the range 400–800 nm and monitoring the change of the 664 nm peak during light irradiation, the intensity of which decreases with MB degradation [39] (UV–Vis-NIR spectrophotometer, Varian Carry 6000i, US). The photocatalytic degradation kinetics were described by a pseudo-first-order model, expressed by Eq. (1):

$$ln(C_0/C) = kt \quad (1)$$

where C_0 stands for the initial MB concentration (10 mg/L), C the MB concentration at time t of irradiation, and k is the first-order rate constant.

2.5. Antibacterial properties under visible-NIR light

The antibacterial activities of the CWCDs were performed on Gram-negative *E. coli* (*E.coli*) under visible-NIR light irradiation (Xenon lamp, Hamamatsu L9588, 200 W). First, an inoculum of *E. coli* (ATCC 25,922) was prepared by adding 10 μl aliquot from an *E. coli* stocked batch in 10 mL of Müller-Hinton broth (Sigma-Aldrich). The inoculum was shaken at 80 rpm at 37 °C overnight. Subsequently, the optical density (OD) of the broth culture was evaluated by measuring the absorption at 600 nm with a cell density meter (Model 40, Fisher Scientific), and the concentration of the bacteria was adjusted in order to obtain a final OD of 0.2, corresponding to ca. 2×10^8 CFU/mL. The stock solution of CWCDs (3 mg/mL) was firstly filtrated with a 0.2 μm cut-off filter to avoid microorganism contamination and ensure the sterility of the samples. Then, CWCDs were diluted in Milli-Q sterile water and subsequently aliquoted inside the 0.2 OD bacterial culture to obtain final concentrations of 56.3, 112.5, 225.0, 450.0, and 600.0 μg/mL in the wells of a 96-well plate. A sample not containing CWCDs but still irradiated with the Xenon lamp under visible-NIR light was used as control. The OD at 0 h of each mixture was measured at 600 nm in a Spark Multimode microplate reader (Tecan Group Ltd., Männedorf, Switzerland). Subsequently, the 96-well plate was irradiated for 30 min of bacterial growth with visible-NIR light emitted from the xenon lamp, at a distance of 17 cm. During the irradiation, the wells were covered with a glass Petri dish to avoid exposure to UV light. Then, the plate was incubated at 37 °C, and after 24 h, the OD at 600 nm was measured for each sample. Triplicate tests were performed in three independent experiments.

Once the optimal concentration at which the CWCDs exerted the higher antibacterial activity was estimated, the effect of the time duration of the irradiation was investigated. The *E. coli* solutions with OD = 0.2 were mixed with the selected concentration (600 μg/mL) of sterile CWCDs and aliquoted in a 96-well plate. The irradiation times used were 0.5, 1, 2, and 3 h. Samples not containing CWCDs but treated with the aforementioned irradiation times were used as control. An extra control was samples that contained CWCDs, but kept in the dark (i.e., no irradiation). The OD at 600 nm was measured as previously described after 24 h. Tests were performed in triplicates, in three independent experiments. Scanning electron microscopy (SEM) was also used to image the bacterial morphology post-irradiation. Briefly, the cells were fixed on a glass coverslip with 2 % glutaraldehyde in 0.1 M sodium cacodylate buffer (pH 7.4, Sigma-Aldrich) for 90 min at room temperature. The fixative solution was subsequently withdrawn, and the samples were washed three times for 10 min each with 0.1 M sodium cacodylate buffer and stored overnight at 4 °C. The samples were post-fixed in 1 % osmium tetroxide (Sigma Aldrich) in 0.1 M sodium cacodylate buffer and then dehydrated in a series of ethanol solutions. Finally, they were incubated in hexamethyldisilazane (HMDS, Sigma-Aldrich) / ethanol solution series, air-dried, sputter-coated with gold, and analyzed by SEM.

2.6. Biocompatibility under visible-NIR light irradiation

Primary human dermal adult fibroblast cells (HDFa, Thermo Fisher Scientific) were used to investigate the *in vitro* biocompatibility of the CWCDs after visible-NIR light irradiation. Following the protocols previously established in our group [40], cells were cultured in T75 culture flasks and were maintained in a humidified incubator with 5 % CO_2 at 37 °C in the presence of fresh Fibroblast Basal Medium supplemented with Supplement Pack Fibroblast Growth Medium 2 (Sigma Aldrich) until 80 % confluency. Afterwards, cells were trypsinized and seeded onto 24-well plates at a density of 7000 cells/cm^2 in 0.5 mL of medium and let attach overnight. The next day the medium was removed, and the fresh one mixed with sterile CWCDs was added, maintaining the final concentration at 600 μm/mL. HDFa mixed with CWCD were kept in the dark or irradiated with visible-NIR light for 1 or 3 h. Cells incubated in normal medium, without CWCDs but irradiated for 3 h, were considered as control. After that, the cells were incubated for additional 24 h. The cell viability was determined via MTS assay: the NAD(P)H-dependent dehydrogenase enzymes in metabolically active cells caused the reduction of the MTS tetrazolium compound and generated the colored formazan product that is soluble in the cell culture media. The color change was recorded via optical density at 490 nm. All assays were performed in triplicates and with three independent experiments.

2.7. Paper sensor for bacteria

PVA:water mixtures (5% w/v) were placed on a hot plate at 90 °C under magnetic stirring until PVA was dissolved. Then, the CWCDs were added at a concentration of 10% w/w. The paper sensors were prepared by dip coating. Briefly, Whatman filter paper was cut in circular pieces (6 mm diameter) and dipped for 10 min in 2 mL of the aforementioned solution. Subsequently, the paper sensors were dried overnight at ambient conditions. For the sensing experiments, 20 μL of bacteria suspended in Müller-Hinton broth (2×10^8 CFU/mL) were placed on the circular filter paper and let dry. Subsequently, the sensors were placed under a UV lamp (emitting at 365 nm) and digital photos were taken.

3. Results and discussion

3.1. Characterization of CWCD

The elemental composition of CWCDs was analyzed by XPS. In Fig. 1a the high resolution XPS scan shows that they are mainly composed of oxygen and carbon, with small contributions of sulphur and nitrogen. Fitting the C1s curve (Fig. 1b) reveals the contributions of sp^2 carbon (C–C, C = C at 284.8 eV), sp^3 carbon (C–O at 286.49 eV) and O–C = O (and C = N—H) at 288.48 eV. In the same spectral region coincide the contributions of sulphur and nitrogen [8,41]. Fitting the O1s peak (Fig. 1c) reveals the contributions of C = O (from the sp^2 carbons at 531.41 eV), S–O (at 532.25 eV) and C–O (at 532.95 eV) [8]. The S_{2p} peak (Fig. 1d) can be fitted by two components arising from –C–SO_x– ($x = 3,4$) species [29]. Finally, the N1s scan (Fig. 1e) shows two nitrogen contributions from pyrrolic N (at 399.78 eV) and graphitic N (at 402.28 eV) [42,43].

Furthermore, Raman investigation of the CWCDs was performed. In Fig. 1f the μRaman spectrum shows two broad peaks, at 1347 cm^{-1} (D peak) and 1546 cm^{-1} (G peak). The D peak is due to the presence of defects in the graphite lattice (sp^3 carbon), while the G peak is due to the sp^2 carbon lattice. The existence of these two peaks indicate the presence

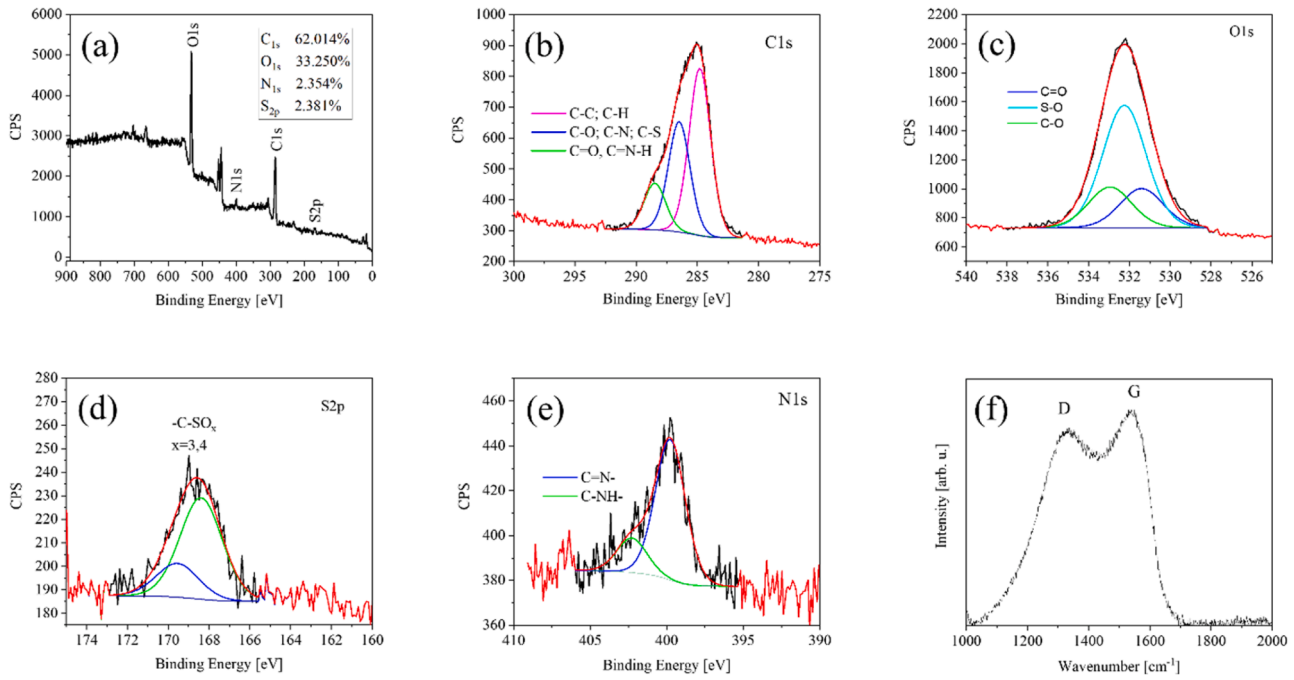

Fig. 1. (a) XPS survey spectrum of CWCDs. The unidentified peaks on the survey spectrum come from the indium substrate. (b) C1s peak fitting. (c) O1s peak fitting. (d) S peak fitting. (e) N peak fitting. (f) Raman spectrum of CWCDs.

of graphitic structure of the CWCDs. The ratio I_D/I_G equals 1.11, indicating a high amount of defects present in the CWCDs [41].

SAXS measurements were performed in order to measure the diameter of CWCDs (Y, SI). At the very low q region, an abrupt increase of the scattering signal is documented, due to the presence of particle aggregates, and was excluded from the fitting. Assuming spherical, carbon particles, the fitting of the experimental curve (after background correction) determines the diameter of the particles to be ca. 1 nm.

TEM imaging (Fig. S2, SI) did not give us concrete results on the morphology of the CWCDs. As becomes obvious from the recent literature, a scientific discussion on the structure and origin of fluorescence of CDs is ongoing, with some authors debating that the fluorescence comes from small molecular byproducts [44–47], rendering TEM analysis insufficient for the CD characterization. In the present study, although we were not able to image tangibly the CWCDs by TEM, we lean on the existence of small particles with graphitic core, as clearly indicated by the existence of the D and G bands in the Raman spectrum and SAXS.

3.2. Optical properties

The absorption spectrum of the aqueous dispersion of CWCDs, shown in Fig. 2a, displays a broad UV absorption at 271 nm and a tail extending into the visible. The first is due to the transition of the aromatic sp^2 domains of the C = C bond, while the second is due to the n-π^* of the C = O bond of the CWCDs [9,48]. In the inset, the photographs of a CWCD aqueous solution are taken under normal lab light (left) and under a UV light of 365 nm (right). The blue colour of the solution in the second case is due to the fluorescence of the CWCDs. Furthermore, the excitation (PLE) and emission photoluminescence (PL) spectra are shown in Fig. 2b. The PLE exhibits two peaks, at 260 nm and 320 nm, indicating two electronic transitions. PL emission from the CWCDs is excitation dependent and the PL peak is redshifting with increasing excitation wavelength (Fig. S3, SI). On excitation with 320 nm, the PL spectrum shows an intense emission centred at 440 nm.

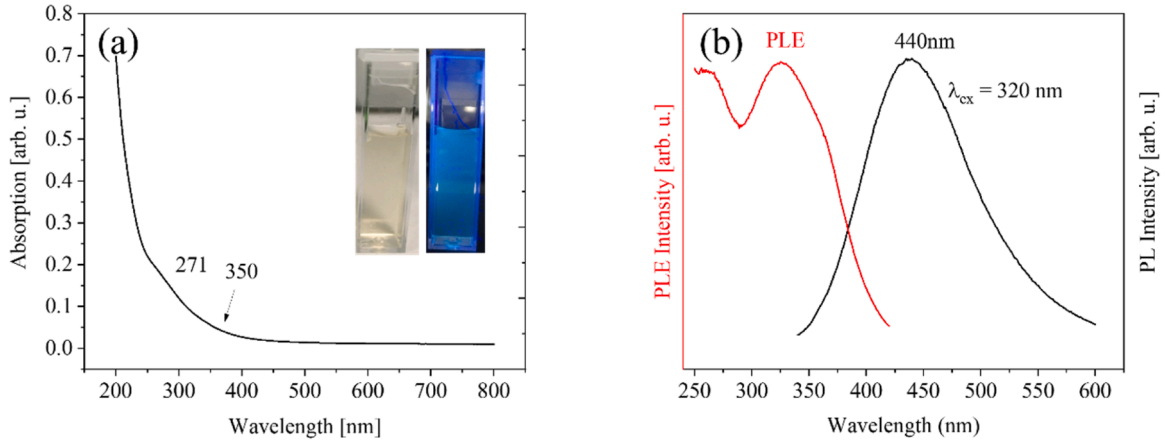

Fig. 2. (a) UV/Vis Absorption spectrum of an aqueous dispersion of CWCDs and photographs under ambient and UV light. (b) PL and PLE of aqueous dispersions of CWCDs.

3.3. Photodegradation of MB under visible-NIR light

The photocatalytic performance of CWCDs under visible-NIR lamp irradiation was investigated by the photodegradation of MB. MB solutions containing different concentrations of CWCD, namely 40 and 600 μg/mL (named CWCD40 and CWCD600, respectively) were tested. Furthermore, a pure MB solution control sample was irradiated under the same conditions, where approximately 17 % of degradation took place, due to intrinsic photolysis [39]. The absorption of the MB-CWCD solution at different irradiation points is shown in Fig. S4 (SI). The photodegradation of MB is much more significant in the presence of CWCD (Fig. 3a), where the photocatalytic efficiency (C/C_0) of CWCDs is shown to depend on their concentration. More specifically, the initial concentration of MB decreases by 40 % in the case of CWCD600 and 35 % for CWCD40, after 360 min of visible light irradiation. It is interesting to note here, that the photocatalytic degradation of MB follows also different kinetics for the two CWCD concentrations. In the case of CWCD600, degradation follows a pseudo-first-order kinetic, as shown in Fig. 3b. However, in the case of CWCD40 the MB degradation curve exhibits an initial delay in the photocatalytic performance for the first 180 min, followed by pseudo-first-order kinetics. Indeed, the first 180 min the photodegradation of the MB follows the same kinetics as the intrinsic MB photolysis. This delay might be due to the slower diffusion of the CWCDs on the sites of action, due to their lower concentration. The photodegradation rate constant (k) was calculated using Eq. (1) to be 0.0014 min^{-1} (R^2=0.990) for CWCD600 and 0.0017 min^{-1} (R^2=0.963) for CWCD40 after the first 180 min.

Upon irradiation of the CWCDs with visible light, photogeneration of electrons and holes takes place. Subsequently, the electrons reduce O_2 to superoxide radicals (O_2^-), while the holes either directly oxidize MB or oxidize H_2O to form hydroxyl radicals (OH•). The CWCDs-induced degradation of MB takes place when redox reactions are initiated by these radical species [15,39].

3.4. Antibacterial properties under visible-NIR light irradiation

The ability of CWCDs to generate ROS species when exposed to visible-NIR light irradiation, as shown from their photocatalytic properties, can directly affect the growth and morphology of bacterial cells in their vicinity. Hence, the antibacterial properties of CWCDs against *E. coli* were investigated. Fig. 4a shows the bacterial growth after visible-NIR irradiation for 30 min in the presence of different CWCD concentrations, and subsequent 24 h of incubation. A bacteria solution without CWCDs (0 μg/mL) was considered as control. Compared to the control sample, no considerable change in bacterial growth is observed for CWCD concentrations up to ca. 400 μg/mL. However, once the concentration of CWCDs reaches 450 μg/mL, the bacterial concentration is decreased by ~11%. The antibacterial action of CWCDs is further increased when their concentration becomes 600 μg/mL, reaching ~33% reduction in bacteria concentration.

Next, using the CWCD concentration that demonstrated the best antibacterial activity upon 30 min irradiation, we performed the antibacterial assay for different irradiation periods (Fig. 4b). The samples were either kept in the dark (sample: CWCD dark), or irradiated for different times, namely 0.5, 1.0, 2.0 and 3.0 h. In the control sample, no CWCDs were added. First, there is a decrease in bacterial concentration with the mere presence of CWCD, even without irradiation, indicating the antibacterial nature of the CWCDs. In comparison to the data obtained in the dark, a stronger antibacterial activity was observed when the samples were irradiated with visible-NIR light. After 0.5 h of visible-NIR light irradiation, there was a decrease of 23.3 %, while over 30.0 % of the *E.coli* cells were killed within 3 h at the same CWCDs dose. The increasing irradiation time, from 0.5 to 3.0 h only minimally enhances the reduction of *E. coli*, and no statistically significant differences were found between these groups.

Furthermore, the effect of CWCDs and visible-NIR light irradiation on the *E. coli* morphology was investigated by SEM. As shown in Fig. 4c, bacteria cells treated in the dark containing CWCDs, exhibit smooth cell walls and clearly defined borders. In contrast, bacteria incubated with CWCD and irradiated for different time durations presented wrinkled and damaged cell surfaces.

The above results evidence that the CWCDs possess antibacterial activity even in the absence of irradiation. Nevertheless, upon irradiation with visible-NIR light their antibacterial activity is significantly enhanced. This is related to the photoinduced redox processes due to the photocatalytic activity under visible-NIR light irradiation (Fig. 3). The morphology of the cells seen at SEM after treatment also indicates that the antimicrobial process includes breaking bacterial cell walls. It is interesting to note here, that although CWCDs are antibacterial even without light irradiation, we have seen cell wall destruction only when bacteria were treated with light. This possibly indicates different antibacterial actions, since the bacteria walls are destroyed only under the action of ROS. However, a more detailed biological analysis would be needed in order to fully understand the different antibacterial actions of CWCDs, with and without light irradiation, which is beyond the scope of this paper.

3.5. Biocompatibility under visible-NIR light irradiation

In order to evaluate the cytotoxicity due to the irradiation with visible-NIR light on human cells, cell viability experiments were carried out *in vitro* for various irradiation periods, using the CWCD

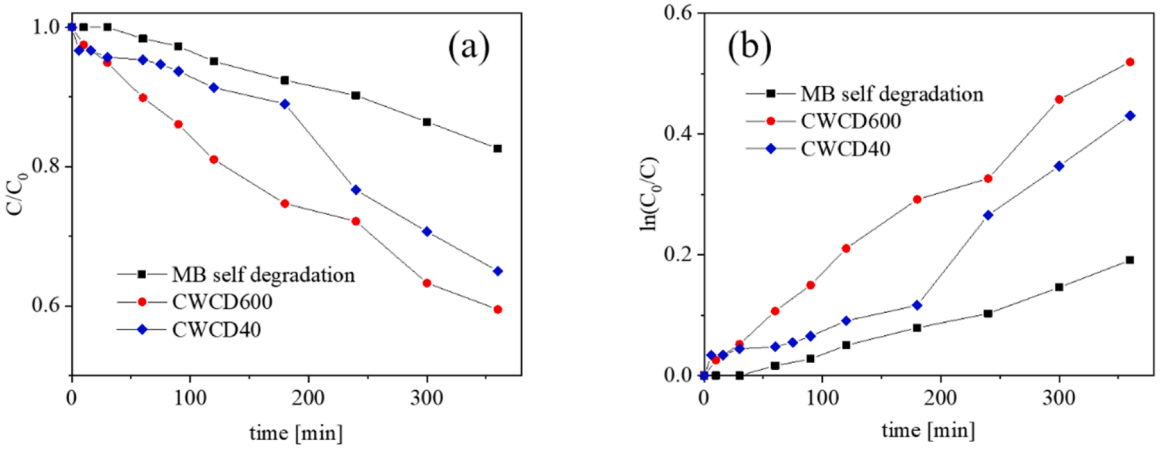

Fig. 3. (a) Photocatalytic degradation efficiency of MB aqueous solutions (10 mg/L) in the presence CWCDs. (b) Kinetics of MB photocatalytic degradation under visible-NIR light.

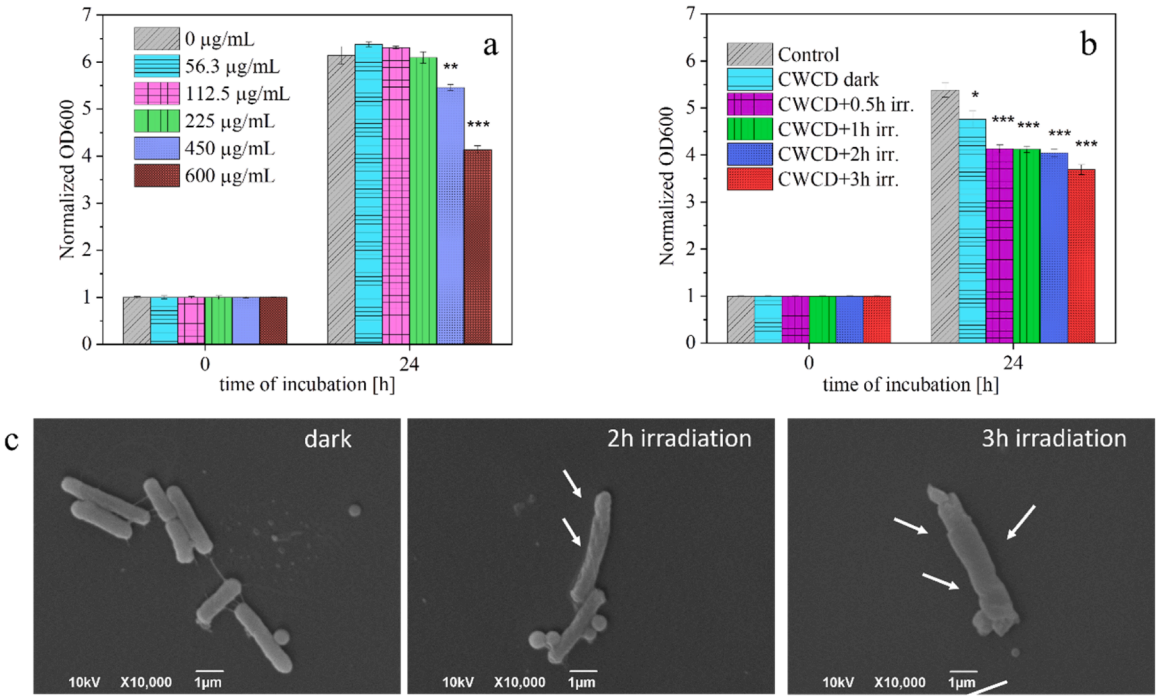

Fig. 4. (a) Inhibition effect of different concentrations of CWCDs on the growth of *E.Coli*. (b) Inhibition effect of different irradiation times on the growth of *E.Coli* with 600 μg/mL CWCDs. (c) SEM images of *E.Coli* cells after treatment with 600 μg/mL CWCDs in the dark and different irradiation times. All results are presented as mean ± standard error of $n = 9$ experimental results for each condition. Significance is expressed in terms of $p < 0.001$ (***), $p < 0.01$ (**), and $p < 0.05$ (*) compared to the control samples.

concentration presenting the highest antibacterial activity upon visible-NIR light irradiation. In this test, human dermal fibroblast (HDFa) cells were used as the *in vitro* model. Fibroblast cultures, containing 600 μg/mL CWCDs, were kept either in the dark or irradiated for 1 or 3 h and subsequently they were incubated for 24 h. As shown in Fig. 5, cells grown in the dark in the presence of 600 μg/mL CWCDs, present a viability of (105.75 ± 3.01)%, i.e., they are completely viable. A small decrease in the viability of cells that were irradiated is observed, with cells reaching (78.77 ± 6.05)% viability for 1 h irradiation and (75.95 ± 4.33)% viability for 3 h irradiation. Hence, a decrease in biocompatibility is observed with increasing irradiation time. However, fibroblast viability remains higher than 70 %, which is above the threshold defined by ISO 10,993–5, indicating that the tested materials have no cytotoxicity activity.

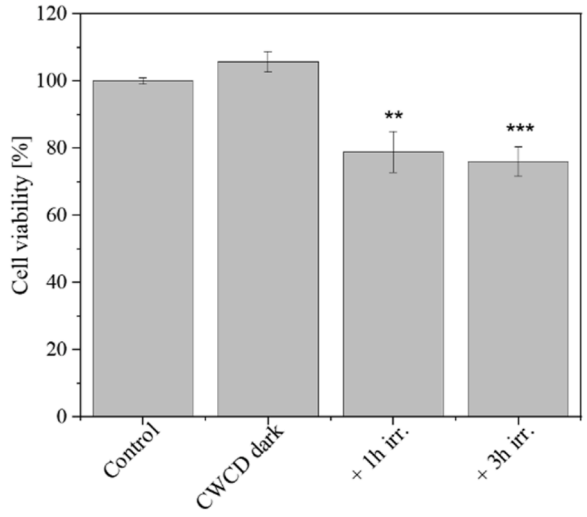

Fig. 5. Biocompatibility tests. Cell viability of HDFa after 24 h incubation with 600 μg/mL CWCDs under different conditions. Cells not receiving any treatment are considered control samples. All results are presented as mean ± standard error of $n = 6$ experimental results for each condition. Significance is expressed in terms of $p < 0.001$ (***) and $p < 0.01$ (**) compared to the control samples.

3.6. Proof-of-concept paper sensor for the detection of E.coli

Based on the fluorescent properties of the CWCDs, we have fabricated paper sensors for the optical detection of bacteria, as a proof-of-concept. Following our previous work [9], we have used PVA/CWCD functionalized paper to detect the presence of *E. coli* by monitoring the fluorescence of the CWCDs in the absence or presence of bacteria. First, filter paper was cut in circular pieces (diameter 6 mm), immersed in PVA/CWCD aqueous solution (10% w/v) for 10 min and left to dry. Fig. 6A shows characteristic photos of the paper samples, functionalized with either pure PVA or PVA/CWCD, taken under UV light (365 nm). Both samples exhibit a blue colour under 365 nm illumination, since also PVA exhibits weak fluorescence upon excitation at this wavelength [49]. In order to enhance the difference in colour due to the fluorescence of CWCDs, we have followed the procedure described in Ref. [9]. By splitting the RGB channels, using the ImageJ software, and applying a colour filter (Lookup Table), different colours appear in channel R for the two samples, as clearly shown in Fig. 6B, as a result of the different fluorescence of the CWCDs in that channel. Subsequently, 20 μl of *E.coli* solutions (2×10^8 CFU/mL) were placed on the paper samples, and they were left for 15–20 min to dry, before new photos were taken under the 365 nm light. In Fig. 6C the photos of the samples display a blue colour similar but not identical to Fig. 6A. Upon further analyzing the photos with ImageJ, the colour of the PVA/CWCD sample matches the one of the PVA sample, indicating the quenching of the fluorescence of the CWCDs.

The quenching of the CDs PL in presence of *E. coli* has been seen in the literature [61] and it was attributed to possible involvement of the CDs surface functional group that can interact with the bacteria. Until

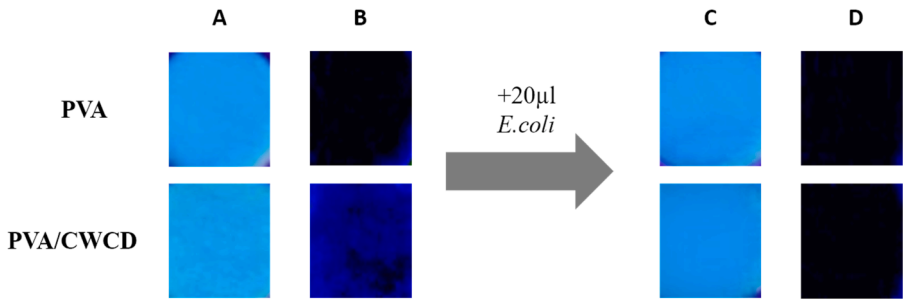

Fig. 6. A: Pristine digital photographs of the paper sensors functionalized with PVA or PVA/CWCDs. B: Processed images of the paper sensors in (A). C: Pristine photographs of the paper sensors after been exposed to *E. coli* bacteria. D: Processed images of the paper sensors in (C).

now, carbon dot fluorescent sensors for bacteria have been presented in their solution form, thus limiting the practical usefulness of the application [50–52]. Sensors based on paper have great advantages in terms of manipulation, transport, and ease of use [53]. The preliminary results of the proof-of-concept test presented here can pave the way to simple and efficient methods for fast detection of the presence of *E.coli* bacteria.

4. Conclusions

We have developed a simple and green procedure to produce highly fluorescent carbon dots (CWCDs) from cotton waste. The resulting CWCDs exhibit strong PL properties. The CWCDs are very stable even after storage for several months and we have used them for MB degradation under visible-NIR light irradiation, showing good photocatalytic properties. They are biocompatible even under visible-NIR light irradiation against human fibroblasts, but show antibacterial activity against Gram-negative bacteria (*E.coli*), which increases upon irradiation with visible-NIR light. Finally, we have produced an optical paper sensor based on the CWCD fluorescence. The fluorescence of the paper sensor is quenched in the presence of *E.coli*, as shown by a simple image analysis. Although the results on the paper sensor are still rather qualitative than quantitative, this proof-of-concept test evidences the potential of the carbon dots, that in conjunction with their antibacterial properties can be used in a range of applications.

Author agreement statement

We the undersigned declare that this manuscript is original, has not been published before and is not currently being considered for publication elsewhere. We confirm that the manuscript has been read and approved by all named authors and that there are no other persons who satisfied the criteria for authorship but are not listed. We further confirm that the order of authors listed in the manuscript has been approved by all of us. We understand that the Corresponding Author is the sole contact for the Editorial process. He/she is responsible for communicating with the other authors about progress, submissions of revisions and final approval of proofs Signed by all authors as follows:

CRediT authorship contribution statement

Evie L. Papadopoulou: Conceptualization, Data curation, Funding acquisition, Investigation, Methodology, Supervision, Validation, Writing – original draft, Writing – review & editing, Project administration. **Aurelio Barbetta:** Conceptualization, Investigation. **Fabrizio Fiorentini:** Investigation, Methodology, Writing – original draft. **Martina Lenzuni:** Investigation, Methodology, Writing – original draft. **Riccardo Carzino:** Investigation. **Silvia Dante:** Investigation. **Luca Leoncino:** Investigation. **Athanassia Athanassiou:** Conceptualization, Funding acquisition, Project administration, Resources, Supervision.

Declaration of competing interest

The authors declare the following financial interests/personal relationships which may be considered as potential competing interests:

Evie L. Papadopoulou reports financial support was provided by National Institute for Insurance against Accidents at Work.

Data availability

Data will be made available on request.

Acknowledgments

This research was part of the Project “Nano and Key enabling technologies within the innovation processes: risk and opportunities in occupational settings by prevention through design (NanoKey Advanced), funded by the Italian Workers’ Compensation Authority (INAIL) and coordinated in cooperation between the INAIL Department of Occupational and Environmental Medicine Epidemiology and Hygiene, and the Italian Institute of Technology (IIT). ELP and LL thank Dr. Rosaria Brescia for useful discussions on TEM. ELP thanks Mr. Giammarino Pugliese and Mr. Simone Nitti for their help on concentrating the carbon dots and Dr. Giulia Biffi for the fruitful discussions.

Supplementary materials

Supplementary material associated with this article can be found, in the online version, at doi:10.1016/j.surfin.2024.104241.

References

[1] X. Xu, et al., Electrophoretic analysis and purification of fluorescent single-walled carbon nanotube fragments, J. Am. Chem. Soc. 126 (40) (2004) 12736–12737.
[2] Y.P. Sun, et al., Quantum-sized carbon dots for bright and colorful photoluminescence, J. Am. Chem. Soc. 128 (24) (2006) 7756–7757.
[3] C. Kang, et al., A review of carbon dots produced from biomass wastes, Nanomaterials 10 (11) (2020) 2316 (Basel).
[4] J. Liu, R. Li, B. Yang, Carbon dots: a new type of carbon-based nanomaterial with wide applications, ACS Cent. Sci. 6 (12) (2020) 2179–2195.
[5] M. Li, et al., Review of carbon and graphene quantum dots for sensing, ACS Sens. 4 (7) (2019) 1732–1748.
[6] Y. Kim, G. Jang, T.S. Lee, New fluorescent metal-ion detection using a paper-based sensor strip containing tethered rhodamine carbon nanodots, ACS. Appl. Mater. Interfaces 7 (28) (2015) 15649–15657.
[7] Q. Wu, et al., Yellow-emitting carbon-dots-impregnated carboxy methyl cellulose/poly-vinyl-alcohol and chitosan: stable, freestanding, enhanced-quenching Cu2+-ions sensor, J. Mater. Chem. C 6 (16) (2018) 4508–4515.
[8] A. Senthamizhan, et al., Hydrochromic carbon dots as smart sensors for water sensing in organic solvents, Nanoscale Adv. 1 (11) (2019) 4258–4267.
[9] E.L. Papadopoulou, et al., Paper sensors based on fluorescence changes of carbon nanodots for optical detection of nanomaterials, Sustainability 13 (21) (2021) 11896.
[10] Y. Wang, et al., Fluorescent polyvinyl alcohol films based on nitrogen and sulfur co-doped carbon dots towards white light-emitting devices, New J. Chem. 40 (10) (2016) 8710–8716.

[11] S. Sahu, et al., Simple one-step synthesis of highly luminescent carbon dots from orange juice: application as excellent bio-imaging agents, Chem. Commun. 48 (70) (2012) 8835–8837.
[12] V.N. Mehta, S. Jha, S.K. Kailasa, One-pot green synthesis of carbon dots by using Saccharum officinarum juice for fluorescent imaging of bacteria (Escherichia coli) and yeast (Saccharomyces cerevisiae) cells, Mater. Sci. Eng. C 38 (2014) 20–27.
[13] K.M. Omer, et al., Carbon nanodots as efficient photosensitizers to enhance visible-light driven photocatalytic activity, J. Photochem. Photobiol. A Chem. 364 (2018) 53–58.
[14] U.A. Rani, et al., Sustainable production of nitrogen-doped carbon quantum dots for photocatalytic degradation of methylene blue and malachite green, J. Water Process Eng. 40 (2021) 101816.
[15] S. Sawalha, et al., Optical properties and photoactivity of carbon nanodots synthesized from olive solid wastes at different carbonization temperatures, RSC Adv. 12 (8) (2022) 4490–4500.
[16] X. Wu, et al., Photodynamic anti-bacteria by carbon dots and their nano-composites, Pharmaceuticals 15 (4) (2022) 487.
[17] C. Zhou, Y. Wang, Recent progress in the conversion of biomass wastes into functional materials for value-added applications, Sci. Technol. Adv. Mater. 21 (1) (2020) 787–804.
[18] X. Wen, et al., Green synthesis of carbon nanodots from cotton for multicolor imaging, patterning, and sensing, Sens. Actuators B Chem. 221 (2015) 769–776.
[19] S. Wu, et al., Large-scale one-step synthesis of carbon dots from yeast extract powder and construction of carbon dots/PVA fluorescent shape memory material, Adv. Opt. Mater. 6 (7) (2018) 1701150.
[20] Z. Wang, et al., Photoluminescent carbon quantum dot grafted silica nanoparticles directly synthesized from rice husk biomass, J. Mater. Chem. B 5 (24) (2017) 4679–4689.
[21] Y. Zhou, et al., Multicolor carbon nanodots from food waste and their heavy metal ion detection application, RSC Adv. 8 (42) (2018) 23657–23662.
[22] C. Wang, et al., Facile synthesis of novel carbon quantum dots from biomass waste for highly sensitive detection of iron ions, Mater. Res. Bull. 124 (2020) 110730.
[23] S. Deshmukh, A. Deore, S. Mondal, Ultrafast dynamics in carbon dots as photosensitizers: a review, ACS. Appl. Nano Mater. 4 (8) (2021) 7587–7606.
[24] M.K. Barman, et al., An efficient charge separation and photocurrent generation in the carbon dot–zinc oxide nanoparticle composite, Nanoscale 9 (20) (2017) 6791–6799.
[25] K. Shen, et al., One-step synthesis of band-tunable N, S co-doped commercial TiO2/graphene quantum dots composites with enhanced photocatalytic activity, RSC Adv. 7 (38) (2017) 23319–23327.
[26] J.B. Essner, G.A. Baker, The emerging roles of carbon dots in solar photovoltaics: a critical review, Environ. Sci. Nano 4 (6) (2017) 1216–1263.
[27] A. Wang, et al., Large-scale synthesis of carbon dots/TiO2 nanocomposites for the photocatalytic color switching system, Nanoscale Adv. 1 (5) (2019) 1819–1825.
[28] A. Bhati, et al., Sunlight-induced photochemical degradation of methylene blue by water-soluble carbon nanorods, Int. J. Photoenergy (2016) 2583821, 2016.
[29] D. Sun, et al., Hair fiber as a precursor for synthesizing of sulfur- and nitrogen-co-doped carbon dots with tunable luminescence properties, Carbon 64 (2013) 424–434.
[30] G. Fu, P.S. Vary, C.T. Lin, Anatase TiO2 nanocomposites for antimicrobial coatings, J. Phys. Chem. B 109 (18) (2005) 8889–8898.
[31] M.R. Khafaga, H.E. Ali, A.W.M. El-Naggar, Antimicrobial finishing of cotton fabrics based on gamma irradiated carboxymethyl cellulose/poly(vinyl alcohol)/TiO2 nanocomposites, J. Text. Inst. 107 (6) (2016) 766–773.
[32] X.L. Dong, W, M.J. Meziani, Y.P. Sun, L. Yang, Carbon dots as potent antimicrobial agents, Theranostics 10 (2) (2020) 15.
[33] M. Ghirardello, J. Ramos-Soriano, M.C. Galan, Carbon dots as an emergent class of antimicrobial agents, Nanomaterials 11 (8) (2021) 1877.
[34] M.J. Meziani, et al., Visible-light-activated bactericidal functions of carbon "Quantum" dots, ACS Appl. Mater. Interfaces 8 (17) (2016) 10761–10766.
[35] M.M. Al Awak, et al., Correlation of carbon dots' light-activated antimicrobial activities and fluorescence quantum yield, RSC Adv. 7 (48) (2017) 30177–30184.
[36] R. Jijie, et al., Enhanced antibacterial activity of carbon dots functionalized with ampicillin combined with visible light triggered photodynamic effects, Colloids Surf. B Biointerfaces 170 (2018) 347–354.
[37] C.Y. Chen, Y.H. Tsai, C.W. Chang, Evaluation of the dialysis time required for carbon dots by HPLC and the properties of carbon dots after HPLC fractionation, New J. Chem. 43 (16) (2019) 6153–6159.
[38] W.S. Rasband. ImageJ, US National Institutes of Health, Bethesda, Maryland, USA, 2024, pp. 1997–2018. https://imagej.nih.gov/ij/.
[39] I. Khan, et al., Review on methylene blue: its properties, uses, toxicity and photodegradation, Water 14 (2) (2022) 242.
[40] F. Fiorentini, et al., Plant-based biocomposite films as potential antibacterial patches for skin wound healing, Eur. Polym. J. 150 (2021) 110414.
[41] J.C. Vinci, et al., Spectroscopic characteristics of carbon dots (C-dots) derived from carbon fibers and conversion to sulfur-bridged C-dots nanosheets, Appl. Spectrosc. 69 (9) (2015) 1082–1090.
[42] Y. Zhang, et al., Solid-state fluorescent carbon dots with aggregation-induced yellow emission for white light-emitting diodes with high luminous efficiencies, ACS Appl. Mater. Interfaces 11 (27) (2019) 24395–24403.
[43] P. Lazar, R. Mach, M. Otyepka, Spectroscopic fingerprints of graphitic, pyrrolic, pyridinic, and chemisorbed nitrogen in N-doped graphene, J. Phys. Chem. C 123 (16) (2019) 10695–10702.
[44] M. Righetto, et al., The elusive nature of carbon nanodot fluorescence: an unconventional perspective, J. Phys. Chem. C 124 (40) (2020) 22314–22320.
[45] I.J. Gómez, et al., Spontaneous formation of carbon dots helps to distinguish molecular fluorophores species, Appl. Surf. Sci. 610 (2023) 155536.
[46] G. Batra, et al., Structural and spectroscopic characterization of pyrene derived carbon nano dots: a single-particle level analysis, Nanoscale 14 (9) (2022) 3568–3578.
[47] S. Khan, et al., Small molecular organic nanocrystals resemble carbon nanodots in terms of their properties, Chem. Sci. 9 (1) (2018) 175–180.
[48] Y. Liu, C.Y. Liu, Z.Y. Zhang, Synthesis and surface photochemistry of graphitized carbon quantum dots, J. Colloid Interface Sci. 356 (2) (2011) 416–421.
[49] J. Mieloszyk, R. Drabent, J. Siódmiak, Phosphorescence and fluorescence of poly (vinyl alcohol) films, J. Appl. Polym. Sci. 34 (4) (1987) 1577–1580.
[50] S. Chandra, et al., One-step synthesis of amikacin modified fluorescent carbon dots for the detection of Gram-negative bacteria like Escherichia coli, RSC Adv. 6 (76) (2016) 72471–72478.
[51] M.M.F. Baig, Y.C. Chen, Bright carbon dots as fluorescence sensing agents for bacteria and curcumin, J. Colloid Interface Sci. 501 (2017) 341–349.
[52] H. Safardoust-Hojaghan, et al., Preparation of highly luminescent nitrogen doped graphene quantum dots and their application as a probe for detection of Staphylococcus aureus and E. coli, J. Mol. Liq. 241 (2017) 1114–1119.
[53] T.H. Ulep, J.Y. Yoon, Challenges in paper-based fluorogenic optical sensing with smartphones, Nano Converg. 5 (1) (2018) 14.